


Cite this: *RSC Adv.*, 2020, 10, 26308

# Synthesis and high-pressure studies of strontium diazenide by synchrotron X-ray diffraction and DFT calculations†

Yue Li,<sup>ab</sup> Huanpeng Bu,<sup>b</sup> Qinglin Wang,<sup>c</sup> Jiani Lin,<sup>ab</sup> Xiaoli Wang,<sup>a</sup> Jianfu Li,<sup>a</sup> Pinwen Zhu<sup>\*b</sup> and Hongyang Zhu<sup>†ab</sup>

In this work, strontium diazenide ( $\text{SrN}_2$ ) was synthesized using strontium azide as a starting material in a Walker-type module under high-pressure and high-temperature conditions. The synthesized  $\text{SrN}_2$  was further studied under high pressure up to 43.2 GPa using *in situ* synchrotron X-ray diffraction to supplement the high-pressure exploration of alkaline earth diazenides. The  $\text{SrN}_2$  underwent a possible phase transition from a tetragonal structure into an orthorhombic structure at 12.0 GPa.  $\text{SrN}_2$  shows anisotropic compressibility due to the orientation of the diazenide anions. The bulk modulus of  $\text{SrN}_2$  is 132.4 (10.2) GPa, which is larger than that of  $\text{Sr}(\text{N}_3)_2$ . The larger bulk modulus of  $\text{SrN}_2$  is attributed to the stronger covalent strength between Sr and N atoms in  $\text{SrN}_2$ , which is confirmed by our theoretical calculations.

Received 25th January 2020

Accepted 6th July 2020

DOI: 10.1039/d0ra00789g

rsc.li/rsc-advances

## Introduction

Metal–nitrogen compounds have attracted extensive attention in recent years due to their outstanding physical and chemical properties including high energy density,<sup>1,2</sup> superior hardness,<sup>3,4</sup> and high luminous efficiency.<sup>5,6</sup> Among them, only the nitride ( $\text{N}^{3-}$ ) and azide ( $[\text{N}_3]^-$ ) based compounds have been known for a long time in spite of the fact that numerous theoretical studies have shown that all-nitrogen anions with different valences might be stable.<sup>7–9</sup> In recent years, the progressive developments of high-pressure synthesis of new materials have greatly expanded the class of metal nitrides and stimulated the study of nitrogen compounds. Several novel nitrides with remarkable properties have been synthesized under high pressure and high-temperature conditions. One type of the compounds consists of nitrogen and noble metals (such as osmium, iridium, or platinum) named metal pernitrides.<sup>3,4,10–12</sup> The other is named alkaline earth diazenide containing alkaline earth metals (such as calcium, strontium, and barium) and nitrogen.<sup>13–17</sup> The alkaline earth diazenides and the metal pernitrides have the same formula of  $\text{MN}_2$ , but the anionic dinitrogen units are not identical. In contrast to metal

pernitrides which contain the pernitride units  $[\text{N}_2]^{4-}$  with N–N single bonds, alkaline earth diazenides incorporate quasi-molecular units  $[\text{N}_2]^{2-}$  with  $\text{N}=\text{N}$  double bonds with two surplus electrons within the antibonding  $1\pi_g^*$  molecular orbital.<sup>11,15,18</sup> Metal diazenides have good conductivities similar to metal. Vajenine *et al.* theoretically calculated interactions of Ba 5d and N 2p and concluded that the significant width of the  $\pi^*$  band is responsible for the metallic nature of the diazenides.<sup>14</sup> Subsequently, Schneider *et al.* confirmed alkaline earth diazenides are of temperature-dependent true metallic behavior by conductivity measurements.<sup>9</sup> Lithium diazenide ( $\text{Li}_2\text{N}_2$ ) exhibits characteristics of both electron conduction and ionic conduction due to the ion pathways and relatively smaller radius of lithium ions.<sup>9</sup>

In 2012, Schneider *et al.* successfully synthesized metal diazenides ( $\text{CaN}_2$ ,<sup>17</sup>  $\text{SrN}_2$ ,<sup>17</sup>  $\text{BaN}_2$ ,<sup>17</sup> and  $\text{Li}_2\text{N}_2$  (ref. 8)) employing the controlled thermal decomposition of the corresponding azides at high-pressure and high-temperature conditions. The phase stabilities, structures, chemical bonding, optical, and electronic properties of metal diazenides have been theoretically predicted under high pressure.<sup>18–21</sup>  $\text{Li}_2\text{N}_2$  has been predicted with density functional theory to have three phase transitions of  $Pmmm \rightarrow Immm \rightarrow Pnma \rightarrow Cmcm$  in the pressure range of 0–100 GPa,<sup>8,22,23</sup> and the nitrogen was polymerized with further compressed to 242 GPa.<sup>23</sup>  $\text{BeN}_2$  were predicted Be and adjacent N connect with covalent bonds to enhance the structural stability using performed using density functional theory.<sup>24</sup> Wessel and Kulkarni *et al.* calculated and found that the bulk moduli of alkaline earth diazenides are smaller than those of the metal pernitrides.<sup>11,15,18,25,26</sup> Although extensive theoretical high-pressure studies on metal diazenides have

<sup>a</sup>School of Physics and Electronic Engineering, Linyi University, Linyi 276005, P. R. China

<sup>b</sup>State Key Lab of Superhard Materials, College of Physics, Jilin University, Changchun 130012, P. R. China. E-mail: hongyangzhu@jlu.edu.cn; zhupw@jlu.edu.cn

<sup>c</sup>Shandong Key Laboratory of Optical Communication Science and Technology, School of Physics Science and Information Technology, Liaocheng University, Liaocheng 252059, P. R. China

† Electronic supplementary information (ESI) available. See DOI: 10.1039/d0ra00789g



been carried out, the experimental high-pressure study of metal diazenides is a challenge and has not been reported due to the difficulty of synthesis of sample and the property of sensitive to moisture.

Therefore, the significance and absence of a high-pressure study of  $\text{SrN}_2$  prompted our endeavor to explore its structural properties under high pressure and compressibility. In this work,  $\text{SrN}_2$  was synthesized by controlled decomposition of  $\text{Sr}(\text{N}_3)_2$  in a Walker-type module under high-pressure and high-temperature conditions. The high-pressure structure and compressibility properties of the synthesized  $\text{SrN}_2$  were investigated by measuring synchrotron angle-dispersive X-ray diffraction (XRD) patterns under high pressure up to 43.2 GPa using a symmetric diamond anvil cell (DAC). The crystal orbital Hamiltonian populations (COHP) and integral crystal orbital Hamiltonian populations (ICOHP) values were calculated to obtain deeper insight into the nature of chemical bonding and bonding strength between metal and N atoms.

## Experimental and theoretical section

### Synthesis of $\text{SrN}_2$

The  $\text{SrN}_2$  was synthesized under high-pressure and high-temperature conditions in a Walker-type module in combination with a 1000 t pressure. MgO-octahedra with edge lengths of 14 mm (14/8 assembly) were used as the pressure medium. Eight tungsten carbide cubes with truncation edge lengths of 8 mm compressed the octahedra  $\text{Sr}(\text{N}_3)_2$  was carefully ground and filled into a cylindrical boron nitride crucible in the glovebox. The process of assembling the sample is given in Fig. S1 in the ESI.† The assembly was pressurized to 9.0 GPa within 214 minutes at room temperature, then heated to 823 K in 30 minutes and held at this temperature for 15 minutes, and then cooled down to ambient temperature in 10 minutes. After that, the pressure was released within 623 minutes. The black metallic bulk  $\text{SrN}_2$  was obtained from the boron nitride crucible and kept in silicone oil as  $\text{SrN}_2$  is highly sensitive to moisture.<sup>17</sup> The synthesized sample is shown in Fig. S2.†

### Synchrotron XRD measurements under high pressure

High-pressure experiments were performed in a symmetric diamond anvil cell with flat anvils of 300  $\mu\text{m}$  in diameter. The synthesized  $\text{SrN}_2$  powders were loaded into a 120  $\mu\text{m}$  diameter sample chamber of a T301 steel gasket which was pre-indented to 70  $\mu\text{m}$  thickness. Pressures were measured by the ruby luminescence method.<sup>27</sup> Silicon oil was chosen as a pressure-transmitting medium as the sample is sensitive to moisture. The *in situ* high-pressure synchrotron XRD experiment was carried out at the 4W2 beamline ( $\lambda = 0.6199 \text{ \AA}$ ) of Beijing Synchrotron Radiation Facility and the average time of a collecting spectrum was 300 seconds. The images were collected by a Pilatus image panel detector.  $\text{CeO}_2$  was used to calibrate the distance and geometric parameters between the sample and the detector. The diffraction patterns were transformed into one-dimensional diffraction angle and diffraction intensity using

Fit2D software. The crystal structure was refined using Rietveld refinements packages of Materials Studio software.

### Theoretical calculations

The electronic structure calculations for the  $\text{SrN}_2$  were performed *via* density functional theory (DFT) within the generalized gradient approximation Perdew–Burke–Ernzerhof (GGA-PBE)<sup>28</sup> as executed in the Vienna *Ab initio* Simulation Package (VASP) code.<sup>29</sup> The projector-augmented wave (PAW)<sup>30</sup> method was performed for Sr  $4p^6 5s^2$  and N  $2s^2 2p^3$  as valence states adopted from the VASP potential library. Plane-wave cutoff energy of 600 eV and appropriate Monkhorst–Pack<sup>31</sup>  $k$ -mesh ( $k$ -point grid of  $0.03 \text{ \AA}^{-1}$ ) was chosen to ensure the convergence of less than 1 meV per atom. The COHP and ICOHP values were calculated using the LOBSTER program.<sup>32</sup>

## Results and discussion

The Fig. 1 shows the refinement of synchrotron XRD pattern of the synthesized  $\text{SrN}_2$  measured at 0.4 GPa, which was indexed with the tetragonal structure ( $I4/mmm$ ,  $Z = 2$ , Fig. 2) based on the positions of nine diffraction peaks using Rietveld refinements packages of Materials Studio software, yielding  $a = b = 3.8187 \text{ \AA}$ ,  $c = 6.279 \text{ \AA}$ , and  $V = 91.56 \text{ \AA}^3$ . These cell parameters are in good agreement with the reported results.<sup>17</sup> The Wyckoff positions of Sr atoms and N atoms are assigned to 2a and 4e, respectively.  $\text{SrN}_2$  structure is occupied by all octahedral voids consisted of the strontium ions with  $[\text{N}_2]^{2-}$  units along  $[001]$ . Each strontium ion is coordinated “end-on” by two and “side-on” by four diazenide units, and each diazenide unit is surrounded by six strontium ions as illustrated in Fig. 2. The distance of the N–N bond is  $1.226 \text{ \AA}$ , which is shorter than that of the Sr–N bond of  $2.528 \text{ \AA}$  and  $2.764 \text{ \AA}$ .

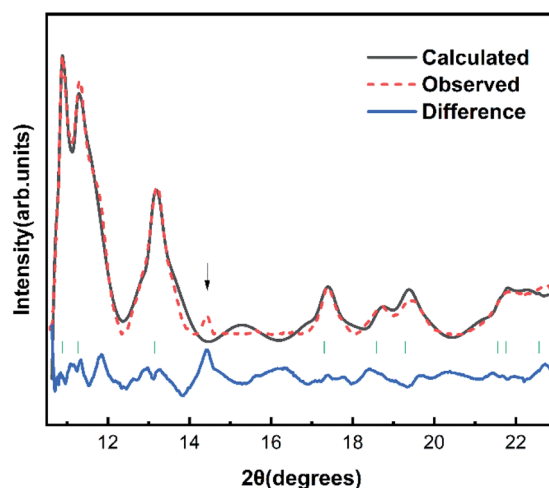


Fig. 1 Rietveld refinement patterns of  $\text{SrN}_2$  at 0.4 GPa with  $R_p = 0.1423$  and  $wR_p = 0.1044$ . The observed data and the simulated profile are provided by the red sphere and black line. The difference curves are shown with a blue line at the bottom. The solid short vertical green lines mark the positions of the Bragg peaks for  $\text{SrN}_2$ . The arrow ( $\downarrow$ ) denotes the diffractions of the  $\text{SrN}_2$  unidentified impurity.

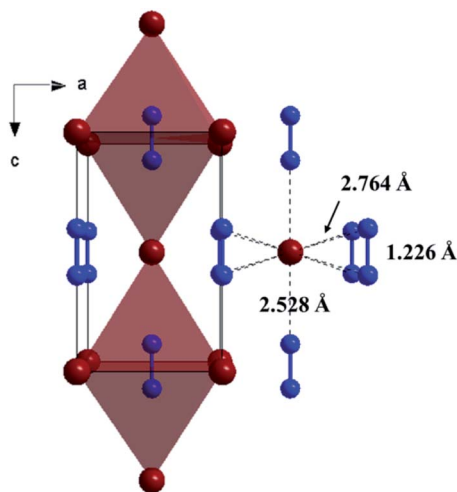


Fig. 2 Crystal structure of the ambient condition tetragonal phase (space group:  $I4/mmm$ ,  $Z = 2$ ) of  $\text{SrN}_2$  along [010]. Red colour represents Sr atoms, and blue colour represents N atoms.

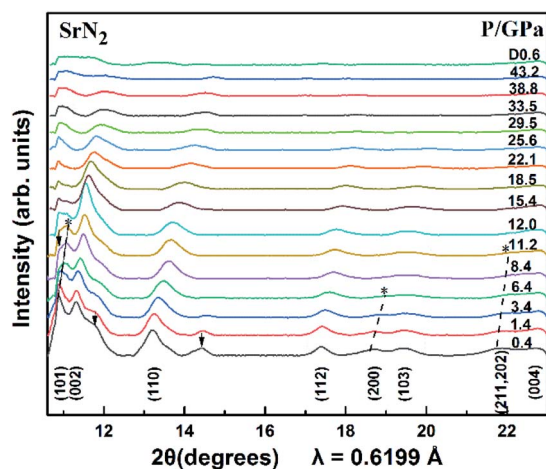


Fig. 3 X-ray diffraction patterns of  $\text{SrN}_2$  at selected pressures ( $\lambda = 0.6199 \text{ \AA}$ ,  $T = 298 \text{ K}$ ). The arrow ( $\downarrow$ ) denotes the diffractions of the  $\text{SrN}_2$  unidentified impurity. The asterisk (\*) denotes the disappearances of the peaks.

The  $\text{SrN}_2$  was compressed up to 43.2 GPa. The XRD patterns are demonstrated in Fig. 3. Nine diffraction peaks of  $\text{SrN}_2$ , which belong to (101), (002), (110), (112), (200), (103), (211), (202), and (004) planes, were observed. The diffraction peaks of (200) disappeared at 6.4 GPa, and (211) and (202) disappeared at 10.0 GPa. The strongest diffraction peak of (101) finally disappeared at 12.0 GPa. The disappearance of the diffraction peaks is temporarily assigned as a possible phase transition. The high-pressure phase is stable up to 43.2 GPa in this study. The peaks of HP- $\text{SrN}_2$  indexing results led to an orthorhombic structure. However, it is difficult to determine the structure of the phase of HP- $\text{SrN}_2$  because the diffraction diagrams are significantly broadened and low intensity at higher pressure. It is worth noting that the detection of the changes of the

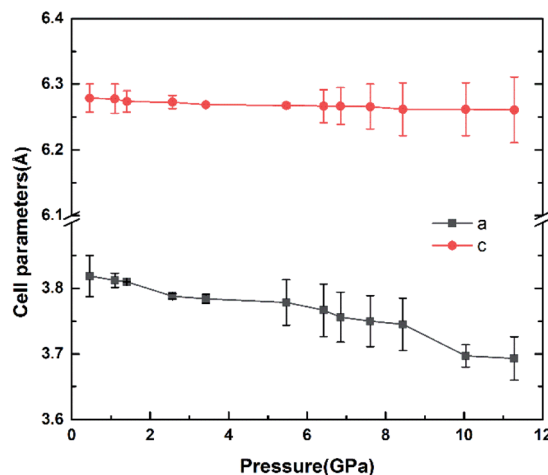


Fig. 4 The cell parameters versus the pressure of  $\text{SrN}_2$ .

diazene anions positions is an inherent challenge for synchrotron XRD measurements owing to their greatly low scattering cross-section. Therefore, a symmetry breaking due to the changes of diazenide anions orientation cannot be observed in synchrotron X-ray diffraction. The similar phenomenon in  $\text{SrO}_2$  was observed.<sup>33</sup> The influence of oxide atoms in  $\text{SrO}_2$  was entirely ignored on the XRD patterns owing to their low scattering cross section. We temporarily ascribe the phase transition of  $\text{SrN}_2$  to the rotation of diazenide units and the rearrangement of Sr ions according to the rotation character of diazenide units in  $\text{CaN}_2$  (ref. 19) under high pressure. As pressure is released to 0.6 GPa, the tetragonal structure recovered from the high-pressure orthorhombic structure, demonstrating a reversible phase transition of  $\text{SrN}_2$ . Compared to the starting conditions, the figure of the back-transformed  $\text{SrN}_2$  shows differences in intensities and is broadened, which are presumably caused by preferred orientation and grain size effects, respectively.

The variation of unit cell lattice parameters of the tetragonal structure with pressure is plotted in Fig. 4.  $\text{SrN}_2$  shows anisotropic compressibility with pressure coefficients of  $1.16 \times 10^{-2} \text{ \AA GPa}^{-1}$  for  $a$ - and  $b$ -axis, and  $1.66 \times 10^{-3} \text{ \AA GPa}^{-1}$  for  $c$ -axis from 0.4 GPa to 11.2 GPa, respectively, which indicates that  $a$ - and  $b$ -axis are more compressive than  $c$ -axis. Analysis of the crystal structure of  $\text{SrN}_2$  reveals that vector projections of repulsive force of diazenides ions are constrained to [001] direction, and without components in [100] and [010] directions as shown in Fig. 2. Therefore, we identify that the orientation of the diazenide anions is the dominant factor that affects the compressibility behaviour of  $\text{SrN}_2$ .

The bulk modulus of  $\text{SrN}_2$  was fitted to the Birch–Murnaghan equation of state (EOS):

$$P = \frac{3}{2}B_0 \left[ \left( \frac{V_0}{V} \right)^{7/3} + \left( \frac{V_0}{V} \right)^{5/3} \right] \times \left\{ 1 + \frac{3}{4} \left( B'_0 - 4 \right) \left[ \left( \frac{V_0}{V} \right)^{2/3} - 1 \right] \right\}, \quad (1)$$



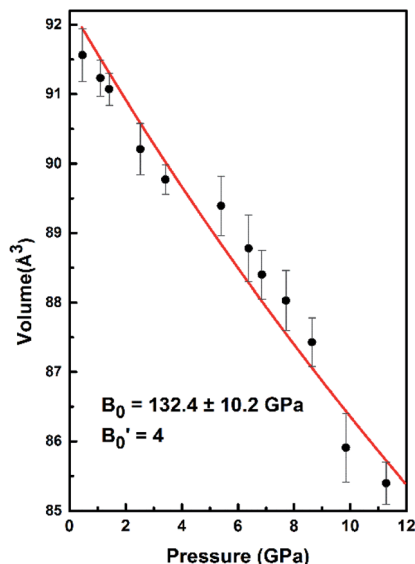


Fig. 5 The volume changes with the pressure for  $\text{SrN}_2$ . The red line exhibits the fitting of data to the Birch–Murnaghan equation of state (EOS).

where  $V_0$  is the unit cell volume at ambient pressure and  $V$  is the volume at the pressure of  $P$ .  $B_0$  is the bulk modulus at zero pressure and  $B'_0$  is the pressure derivative of  $B_0$ . The data measured below 11.2 GPa were used to yield the bulk modulus because the phase transitions occur at 12.0 GPa. The bulk modulus of  $B_0 = 132.4$  (10.2) GPa of  $\text{SrN}_2$  is conforming to the Birch–Murnaghan EOS. The bulk modulus of  $\text{SrN}_2$  is close to that of  $\text{CaN}_2$  (113.2 GPa),<sup>21</sup> which can be interpreted by the fact that  $\text{SrN}_2$  and  $\text{CaN}_2$  are isostructural at ambient conditions. The experimental pressure evolutions of the unit cell volume of  $\text{SrN}_2$  are plotted in Fig. 5. The bulk modulus of  $\text{SrN}_2$  was theoretically predicted to be 96.08 GPa and 65 GPa using pseudo-atomic calculations with the local density approximation (LDA) and the generalized gradient approximation Perdew–Burke–Ernzerhof (GGA-PBE), and the *ab initio* calculations with the GGA-PBE, respectively, by Zhang *et al.*<sup>20</sup> and Wessel *et al.*,<sup>15</sup> in which the pseudo-atomic calculations results are closer to the experimental results. The different calculation methods employed different empirical or theoretical approximations are suitable for different materials. Compare our experimental results with reported calculations results, the pseudo-atomic calculations with the LDA and the GGA-PBE were better fitted diazenides than the *ab initio* calculations with the GGA-PBE. The bulk modulus of  $\text{SrN}_2$  is two times larger than its corresponding metal azide  $\text{Sr}(\text{N}_3)_2$  (123.7 GPa of  $\text{SrN}_2$  vs. 49.1 GPa of  $\text{Sr}(\text{N}_3)_2$  (ref. 34)). The nitrogen bonds are formed as double bonding in both diazenides anions  $(\text{N}=\text{N})^{2-}$  and azides anions  $(\text{N}=\text{N}=\text{N})^-$ .<sup>11</sup> The previous studies proved that the  $\text{N}=\text{N}$  plays a crucial role in the compressibility of both  $\text{Sr}(\text{N}_3)_2$  and  $\text{SrN}_2$ . The  $\text{N}=\text{N}$  bond distance of 1.226 (3) Å in  $\text{SrN}_2$  is longer than that of 1.184 (2) Å in  $\text{Sr}(\text{N}_3)_2$  leading to weaker  $\text{N}=\text{N}$  bonds in  $\text{SrN}_2$ . The bulk modulus of  $\text{SrN}_2$  is larger than that of  $\text{Sr}(\text{N}_3)_2$ , which contradict to the longer  $\text{N}=\text{N}$  bond of  $\text{SrN}_2$ . We thus infer the interaction

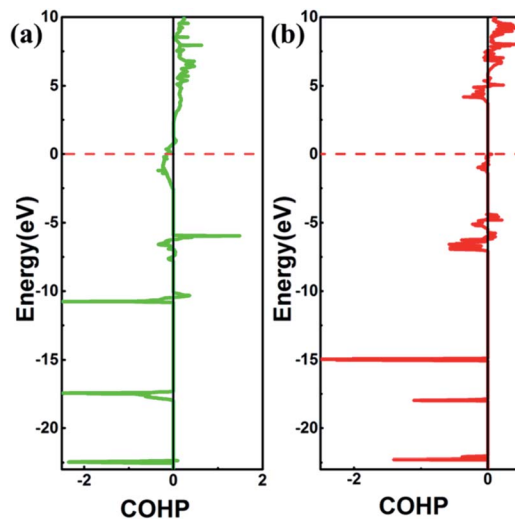


Fig. 6 The plot of COHP for (a)  $\text{SrN}_2$ , Sr1–N1 pairs separated by 2.528 Å (b)  $\text{Sr}(\text{N}_3)_2$ , Sr2–N2 pairs separated by 2.628 Å. The positive and negative COHP values denote antibonding and bonding interactions, respectively.

between Sr and N in  $\text{SrN}_2$  is much stronger than that in  $\text{Sr}(\text{N}_3)_2$ . To obtain deeper insight into the nature of chemical bonding between Sr and N in  $\text{SrN}_2$  and  $\text{Sr}(\text{N}_3)_2$ , we performed crystal orbital overlap population (COHP) analysis. COHP can divide the band-structure energy into the orbital pair interactions, which is used to indicate the contribution of bonding, nonbonding, and antibonding to the band-structure energy. Our analysis showed that bonding states are fully occupied and antibonding states are partially occupied in  $\text{SrN}_2$ , while both bonding states and anti-bonding states are partially occupied in  $\text{Sr}(\text{N}_3)_2$ , as shown in Fig. 6, leading to strong covalent bonding between Sr and N atoms in  $\text{SrN}_2$  and  $\text{Sr}(\text{N}_3)_2$ . Furthermore, the bonding strength can be expressed by the values of integrated crystal orbital Hamilton population (ICOHP), which are in the order of  $-1.233$  and  $-0.736$  for  $\text{SrN}_2$  and  $\text{Sr}(\text{N}_3)_2$ , respectively, as shown in Fig. 6. It is confirmed that interaction between Sr1–N1 atoms is stronger than that of Sr2–N2 atoms. Hence, covalent bonding between Sr and N atoms is stronger in  $\text{SrN}_2$ , which resulted in a larger bulk modulus.

## Conclusions

In this work, the  $\text{SrN}_2$  was synthesized by using the controlled decomposition of the  $\text{Sr}(\text{N}_3)_2$  under high-pressure and high-temperature conditions. The high-pressure *in situ* synchrotron XRD study of the synthesized  $\text{SrN}_2$  up to 43.2 GPa revealed a pressure-induced tetragonal-to-orthorhombic phase transition at 12.0 GPa due to the rotation of diazenide units and the rearrangement of Sr ions. The compressibility of  $\text{SrN}_2$  is anisotropic due to the orientation of the diazenide anions. The bulk modulus of  $\text{SrN}_2$  is  $B_0 = 132.4$  (10.2) GPa. In order to further analyze the bulk modulus of  $\text{SrN}_2$  and  $\text{Sr}(\text{N}_3)_2$ , we calculated the bonding strength *via* computing the values of ICOHP, which shows stronger Sr–N covalent bonds in  $\text{SrN}_2$  than



that in  $\text{Sr}(\text{N}_3)_2$ , leading the larger value of bulk modulus than that of  $\text{Sr}(\text{N}_3)_2$ .

## Conflicts of interest

There are no conflicts to declare.

## Acknowledgements

This work is supported by the National Natural Science Foundation of China (11774128, 11674144, 11604133) and the Natural Science Foundation of Shandong Province (ZR2018JL003, 2019KJJ003, JQ201602, and ZR2018MA038). The high-pressure synchrotron XRD measurements were performed at the Beijing Synchrotron Radiation Facility (BSRF).

## Notes and references

- 1 C. Zhang, C. Sun, B. Hu and M. Lu, *Science*, 2017, **355**, 374.
- 2 M. I. Eremets, R. J. Hemley, H. K. Mao and E. Gregoryanz, *ChemInform*, 2001, **32**, 170–174.
- 3 E. Gregoryanz, C. Sanloup, M. Somayazulu, J. Badro, G. Fiquet, H. K. Mao and R. J. Hemley, *Nat. Mater.*, 2004, **3**, 294–297.
- 4 J. C. Crowhurst, A. F. Goncharov, B. Sadigh, C. L. Evans, P. G. Morrall, J. L. Ferreira and A. J. Nelson, *Science*, 2006, **311**, 1275–1278.
- 5 P. Pust, V. Weiler, C. Hecht, A. Tücks, A. S. Wochnik, A. K. Henß, D. Wiechert, C. Scheu, P. J. Schmidt and W. Schnick, *Nat. Mater.*, 2014, **13**, 891–896.
- 6 P. Pust, P. J. Schmidt and W. Schnick, *Nat. Mater.*, 2015, **14**, 454.
- 7 K. O. Christe, W. W. Wilson, J. A. Sheehy and J. A. Boatz, *Angew. Chem., Int. Ed.*, 1999, **38**, 2004–2009.
- 8 S. B. Schneider, R. Frankovsky and W. Schnick, *Angew. Chem., Int. Ed.*, 2012, **51**, 1873–1875.
- 9 R. Frankovsky, G. M. Friederichs, S. B. Schneider, W. Schnick, M. Mangstl and J. Schmedt auf der Gönne, *Chem. Mater.*, 2013, **25**, 4149–4155.
- 10 Z. W. Chen, X. J. Guo, Z. Y. Liu, M. Z. Ma, Q. Jing, G. Li, X. Y. Zhang, L. X. Li, Q. Wang, Y. J. Tian and R. P. Liu, *Phys. Rev. B: Condens. Matter Mater. Phys.*, 2007, **75**, 1–4.
- 11 M. Wessel and R. Dronskowski, *J. Am. Chem. Soc.*, 2010, **132**, 2421–2429.
- 12 J. C. Crowhurst, A. F. Goncharov, B. Sadigh, J. M. Zaug, D. Aberg, Y. Meng and V. B. Prakapenka, *J. Mater. Res.*, 2008, **23**, 1–5.
- 13 G. Auffermann, Y. Prots and R. Knierp, *Angew. Chem., Int. Ed.*, 2001, **40**, 547–549.
- 14 G. V. Vajenine, G. Auffermann, Y. Prots, W. Schnelle, R. K. Kremer, A. Simon and R. Knierp, *Inorg. Chem.*, 2001, **32**, 4866–4870.
- 15 W. Michael and D. Richard, *J. Comput. Chem.*, 2010, **31**, 1613–1617.
- 16 G. Auffermann, R. Knierp and W. Bronger, *Z. Anorg. Allg. Chem.*, 2006, **632**, 565–571.
- 17 S. B. Schneider, R. Frankovsky and W. Schnick, *Inorg. Chem.*, 2012, **51**, 2366–2373.
- 18 A. Kulkarni, J. C. Schön, K. Doll and M. Jansen, *Chem.-Asian J.*, 2013, **8**, 743–754.
- 19 H. Wang, Y. Yao, Y. Si, Z. Wu and G. Vaitheeswaran, *J. Phys. Chem. C*, 2014, **118**, 650–656.
- 20 L. Q. Zhang, Y. Cheng, Z. W. Niu, C. G. Piao and G. F. Ji, *Z. Naturforsch., A: Phys. Sci.*, 2014, **69**, 619–628.
- 21 S. Xu, L. Zhang and Y. Cheng, *J. Wuhan Univ. Technol., Mater. Sci. Ed.*, 2016, **32**, 100–105.
- 22 Y. Shen, A. R. Oganov, G. Qian, J. Zhang and H. Dong, *Sci. Rep.*, 2015, **5**, 14204.
- 23 J. Zhang, X. Wang, K. Yang, Y. Cheng and Z. Zeng, *Sci. Rep.*, 2018, **8**, 13144.
- 24 J. Lin, Z. Zhu, Q. Jiang, S. Guo, J. Li, H. Zhu and X. Wang, *AIP Adv.*, 2019, **9**, 055116.
- 25 R. Yu, Q. Zhan and L. C. De Jonghe, *Angew. Chem., Int. Ed.*, 2007, **46**, 1136–1140.
- 26 M. Wessel and R. Dronskowski, *Chem.-Eur. J.*, 2011, **17**, 2598–2603.
- 27 H. K. Mao, J. Xu and P. M. Bell, *J. Geophys. Res.*, 1986, **91**, 4673–4676.
- 28 J. P. Perdew, K. Burke and M. Ernzerhof, *Phys. Rev. Lett.*, 1996, **77**, 3865–3868.
- 29 G. Kresse and J. Furthmüller, *Phys. Rev. B: Condens. Matter Mater. Phys.*, 1996, **54**, 11169–11186.
- 30 P. E. Blochl, *Phys. Rev. B: Condens. Matter Mater. Phys.*, 1994, **50**, 391–396.
- 31 H. J. Monkhorst, *Phys. Rev. B: Condens. Matter Mater. Phys.*, 1976, **13**, 5188–5192.
- 32 S. Maintz, V. L. Deringer, A. L. Tchougréeff and R. Dronskowski, *J. Comput. Chem.*, 2016, **37**, 1030–1035.
- 33 Y. Wang, S. Wang, Y. Zhang, J. Lv, Y. Chen, W. Zheng and Y. Ma, *Inorg. Chem.*, 2017, **56**, 7545–7549.
- 34 H. Zhu, X. Han, P. Zhu, X. Wu, Y. Chen, M. Li, X. Li and Q. Cui, *J. Phys. Chem. C*, 2016, **120**, 12423–12428.

